scientific reports

Check for updates

OPEN

Structural and textural characterization of *Brassica carinata* biochar to investigate its potential industrial applications

Zinnabu Tassew Redda[1,2]✉, Carsten Prinz[3], Abubeker Yimam[2], Mirko Barz[1], Katharina Becker[4], Desta Getachew Gizaw[5,6] & Asnakech Laß-Seyoum[1]

Biochar, a low-cost, and carbon-rich product of the thermal decomposition of biomass under oxygen-limited conditions and at relatively low temperatures, has recently been identified as a promising porous material with a wide range of industrial applications. In the present study, a comprehensive analysis of proximate, ultimate, nutrient profile, structural, and textural properties of a biochar derived from two Ethiopian indigenous *Brassica carinata* cultivars was conducted. The characterization of the biochar was achieved by employing a variety of well-established methods, including proximate analysis (moisture, volatile matter, ash content, and fixed carbon), ultimate analysis (C, S, and O content), atomic oxygen to carbon ratio (O/C), morphological and elemental composition analysis through scanning electron microscopy coupled with energy-dispersive X-ray spectroscopy (SEM-EDS). Furthermore, a combination of mercury intrusion porosimetry (MIP), dynamic vapor sorption (DVS), and gas adsorption methods such as nitrogen and krypton gas adsorption, were used for an in-depth study of the porous structure. SEM morphological characterization showed that the biochar surfaces showed multiple pores of diverse sizes and shapes. EDS elemental composition analysis revealed that sodium, aluminium, and silicon were not detected, but potassium, calcium, magnesium, and iron were all present in noticeable amounts. Furthermore, ultimate analysis showed that the most prevalent elements were carbon (86 wt.%) and oxygen (10.41–9.77 wt.%), while sulphur was present in negligible concentrations. MIP analysis demonstrated that the porosities of the biochars varied from 62.68 to 69.99 wt.%, with the Holetta-1 biochar showing the highest porosity. The superior porosity of Holetta-1, as confirmed via MIP analysis, yielded higher values for bulk volume (2.36 mL g^{-1}), skeletal volume (1.65 mL g^{-1}), and total intrusion volume (1.65 mL g^{-1}) compared to the Yellow Dodolla. The most frequent pore diameters were 172.46 µm for Yellow Dodolla and 111.42 µm for Holetta-1. The MIP log differential pore diameter distributions were observed to vary from 18 to 411 µm and 10 to 411 µm, respectively, for Yellow Dodolla and Holetta-1. Despite the biochars' low specific surface areas (0.17–0.21 m^2 g^{-1}), krypton sorption was a suitable technique for its characterization compared to DVS and nitrogen sorption methods. In conclusion, the characterization studies confirmed that this carbon-rich porous material possesses unique and valuable properties, with these attributes position it as a promising alternative for diverse industrial applications, contributing to the development of a bio-based circular economy.

Keywords Morphological characterization, Mercury intrusion porosimetry, Porosity, Gas adsorption, Specific surface area, Nitrogen gas adsorption, Krypton gas adsorption, BET analysis

[1]Faculty 1, University of Applied Sciences (HTW) Berlin, Wilhelminenhofstraße 75A, 12459 Berlin, Germany. [2]School of Chemical and Bio Engineering, College of Technology and Built Environment (Former: Addis Ababa Institute of Technology), Addis Ababa University (AAU), King George VI St., 385, Addis Ababa, Addis Ababa, Ethiopia. [3]Department of Structural Analysis, Federal Institute for Materials Research and Testing (BAM), Richard-Willstätter-Straße 11, 12489 Berlin, Germany. [4]Faculty 2, University of Applied Sciences (HTW) Berlin, Wilhelminenhofstraße 75A, 12459 Berlin, Germany. [5]Department of Environmental Engineering, National Cheng Kung University, Tainan 70101, Taiwan. [6]Department of Chemical Engineering, School of Mechanical, Chemical and Materials Engineering, Adama Science and Technology University, Adama 1888, Ethiopia. ✉email: zinnabu.tassew@aau.edu.et

Abbreviations

ASAP	Accelerated surface area and porosimetry
AC	Total ash content
BET	Brunauer-Emmett-Teller
B. carinata	*Brassica carinata*
DVS	Dynamic vapor sorption
EDS	Energy-dispersive X-ray spectroscopy
FC	Fixed carbon
ISO	International organization for standardization
IUPAC	International union of pure and applied chemistry
Kr	Krypton gas
MC	Moisture content
MIP	Mercury intrusion porosimetry
O/C	Atomic oxygen-to-carbon
PSD	Pore size distribution
S_{BET}	Specific BET surface area
SEM	Scanning electron microscope
SSA	Specific surface area
VM	Volatile matter

Inconceivable population increase and human-induced changes have led to the production of huge volumes of recyclables, a scarcity of natural resources, an overwhelming amount of environmental degradation, and an increased pace of climate change. In recent years, biochar has emerged as a critical strategy for mitigating the severity of these problems. Biochar is a solid carbon-containing material produced through the thermal treatment of biomass-based materials in an oxygen-limited environment[1]. Thermochemical conversion techniques are among the most extensively used biomass valorisation technologies[2]. Torrefaction, gasification, pyrolysis, hydrothermal/flash carbonization, and other processes can be utilized to produce it from agricultural, kitchen, forest, and industrial wastes, or wastes obtained from animals (allowing waste control)[1].

Because of its remarkable qualities, biochar has sparked considerable interest in a variety of disciplines, including agriculture, the environment, and energy [3]. It has been used, particularly, in soil amendment[4,5], adsorption[6,7], energy storage[8–10], catalysis[7,11,12], and compositing[13,14]. Agricultural ecosystems have been proven to benefit from biochar in a wide range of methods, including enhanced yields, better water retention, higher nutrient recycling and retention, greater microbial activity, and higher soil organic matter content[15]. In addition, the incorporation of biochar into soil has substantial advantages, including enhanced physicochemical and biological qualities, soil fertility and crop yield improvement[16], plant disease management [17], as well as harmful metals and organic contaminants immobilization[18]. Biochar also boosts soil microbial population and microbe activity while increasing soil nutrient availability, cation exchange capacity, and water retention capacity[19,20].

The presence of certain types of surface functional groups in biochars may be used, among other things, in the processes of eliminating different pollutants from the environment, such as heavy metals from water or wastewater[21]. In comparison to biochars formed from pyrolysis at a temperature of 673 K, the intensity of surface functional groups was noticeably lower in the case of biochars produced at a temperature of 973 K. The inclusion of particular functional groups can make up for the small specific surface area and improve the sorption characteristics[22].

Biochars have a wide range of physical and chemical features[23], which have a significant impact on their potential utilization throughout the various agricultural and manufacturing industries. The properties of the biochar, such as the elemental compositions, density, porosity, and pH, as well as the process employed for producing the biochar, are greatly influenced by the feedstock and the method used to produce the biochar. These qualities together have an impact on the acceptability of biochar for various uses[24]. Density and porosity, in particular, constitute significant physical characteristics that govern how biochar moves across the landscape and interacts with water to influence soil hydrologic processes, notably plant-available water-holding capacities[25].

It is challenging to accurately characterize the pore structure and pore size distribution of biochars because their pore sizes vary at least five orders of magnitude, from sub-nanometer slit-shaped pores corresponding to spaces between flat aromatic carbon clusters that resemble graphite layers[26,27], to pores on the order of tens of micrometers from partly unaffected cellular structures[28,29]. There is no unique approach that can accurately determine pore volume throughout these scales, hence effective biochar porosity characterization has remained challenging.

As a result of their relative simplicity of use and established relation to chemical sorbate sorbent interactions, gas sorption techniques have become prominent to measure the porosity of carbon materials[30]. Although employing nitrogen gas (N_2) at 77 K is still one of the most widely employed adsorptive in such analyses because of its accessibility, study findings have found that it lacks key essential characteristics for reliable isotherm measurement and the identification of textural parameters[31]. It is generally known that pores with widths comparable to that of N_2 molecules are typical in the case of porous carbons as well as other porous materials such as conjugated microporous polymers (CMPs). This can result in insufficient N_2 diffusion into those pores when applied as an adsorptive gas[32–34].

Krypton gas (Kr) adsorption is a reliable method for measuring specific surface area (S_{BET}). Due to Kr's lower saturation vapor pressure than N_2 and hence smaller sample tube free-space error, it is typically utilized for materials with S_{BET} below that which can be measured by N_2 adsorption. However, some instrumentation modification is frequently required to enable the generation and monitoring of the lower absolute pressures

necessary by Kr adsorption. Kr adsorption can be readily carried out at the same cryogenic temperature used for N_2 adsorption[35].

Mercury intrusion porosimetry (MIP) is another essential approach utilized by many researchers to examine and characterize the pore structure of solid materials because of its simple principle, rapid test speed, and broad pore size measurement range[36]. The MIP is a powerful pore characterization technique that measures a wide variety of pores from a few nanometers to a few hundred micrometers in diameter, in particular, sizes ranging from 500 μm to 3.5 nm in a single analysis that typically lasts between 30 and 45 min [37,38]. Furthermore, according to earlier research, mercury porosimetry can detect more biochar pore volumes than gas sorption does[37].

However, it has some disadvantages, such as the potential for sample crushing under the high pressures required for analysis, which could introduce errors in the porosity measurements, and its inability to distinguish between inter-particle and intraparticle porosity, particularly for powdered samples [37]. Aside from the destructive nature of the analysis approach, there are additional restrictions on safety and mercury handling[37]. Unlike inter-particle analysis, which involves the incursion of mercury between pores, this method of pore structure characterization involves forcing mercury into the pores.

A notable gap in the literature pertains to an in-depth characterization of biochar derived from *Brassica carinata* oilseed meals. The analyses of its proximate, ultimate, atomic oxygen to carbon ratio, morphological, nutrient composition, and textural properties remain markedly unaddressed. The objective of the present study was to conduct a thorough analysis including: the proximate analysis (total moisture, total ash, volatile matter, and fixed carbon); ultimate analysis (C, S, and O content); atomic oxygen to carbon ratio (O/C); morphological and nutrient composition analysis using scanning electron microscopy coupled with energy-dispersive X-ray spectroscopy (SEM-EDS); and mercury intrusion porosimetry (MIP) analysis to determine bulk density, skeletal density, bulk and skeletal (pore) volumes, pore diameter, pore diameter distribution, porosity, total intrusion volume, and total pore area. The characterization study also includes an analysis of the BET specific surface area using dynamic vapor sorption (DVS) and gas adsorption methods such as nitrogen gas (N_2) and krypton gas (Kr) adsorption. Subsequent to this in-depth characterization, the valorization of this agricultural product was studied to explore its promising industrial applications.

Methods

Chemicals and materials

For the present investigation, two *Brassica carinata* oilseed crops—Yellow Dodolla and Holetta-1—were collected from the Holetta Agricultural Research Centre in Holetta, Ethiopia. The collection and use of this plant species was done in accordance with all the relevant guidelines. These Ethiopian indigenous oilseed crops were used in our prior investigations[39,40] to study their promising industrial applications. As detailed in the subsequent section, the oilseed meal—a by-product of solvent extraction of these crops—was converted into biochar using a slow pyrolysis[41]. The present study then focused on characterizing this biochar and assessing its promising industrial applications.

To maintain consistency, the designations for oilseed meal and biochar derived from the same cultivar (e.g., Yellow Dodolla) are used throughout the document (e.g., Yellow Dodolla oilseed meal and Yellow Dodolla biochar). A similar naming was used for Holetta-1 samples. Moreover, krypton gas (Kr, 99.99%, Air Liquide Deutschland GmbH), liquid mercury (Hg, 99.99%, GMR Gesellschaft für Metallrecycling mbH), and nitrogen gas (N_2, 99.999%, Linde GmbH) were the principal analytical components utilized for textural analysis. Further information regarding the oilseed meals and the corresponding pyrolysis yield of biochar and other relevant information is presented in our previously reported investigations[40,41]. Throughout this document, meal refers to oilseed meal and *B. carinata* refers to *Brassica carinata*.

Analytical methods

In the following sections, the pertinent thermochemical conversion of the meals into biochar and the subsequent characterization of the biochar are addressed. Additionally, a variety of analytical techniques, including proximate analysis, morphological analysis, elemental analysis, and textural property quantification, were applied to thoroughly explore the biochar's characterisation properties. In addition to BET specific surface area analysis, the latter approach covers skeletal density, bulk density, total pore volume, porosity, pore size, and pore size distributions.

Thermochemical conversion of B. carinata meals

The present study, which continues our previous examination into the thermochemical conversion of the hexane-defatted *B. carinata* meals[41], emphasizes principally on an in-depth examination of the resulting biochar. This prior paper has shown that pyrolysis, a thermochemical conversion of this biomass material, produced a variety of valuable products, such as bio-oil, biochar, and a mixture of gases mainly syngas. As described in the later sections of the study, the biochar in particular has become a product of great interest because of its versatility for an array of uses. This emphasis stems from the necessity to comprehend the characteristics of the biochar in order to maximize its use and support the circular bioeconomy by transforming a plentiful waste stream into an invaluable resource.

Consequently, this study focuses on characterizing the biochar produced from this meal. The right thermochemical conversion parameters, including temperature and heating rate[41], play an important role for the biochar to gain its characteristics, as detailed in the subsequent sections. This rigorous characterization has maximized the biochar's viability as a sustainable and profitable resource by offering valuable insights into the method of conversion as well as a vital reference for customizing the biochar's characteristics for particular uses.

Proximate analysis of B. carinata biochar

Proximate analysis was conducted to provide the composition in terms of total moisture content (MC), total ash content (AC), volatile matter (VM), and fixed carbon (FC). The MC and AC of char samples were measured, respectively, in an oven (Memmert GmbH + Co.KG, Schwabach, Germany) and furnace (L5/C6, Nabertherm GmbH, Germany), using the standard test technique for chemical analysis of wood charcoal (ASTM D1762-84(2021)). The VM of the samples was evaluated utilizing the standard test method for the chemical analysis of wood charcoal, ASTM D1762-84(2021). This procedure was executed using a muffle furnace (L5/C6, Nabertherm GmbH, Germany). During the execution of this test, the crucibles were covered with lids during testing to mitigate the loss of volatile constituents and to exclude atmospheric oxygen from the process. Equation 1, as indicated below, was used to calculate the VM of the samples. The FC, on the other hand, was calculated by the difference as shown in Eq. (2).

$$VC\ (wt.\%) = \frac{W_1 - W_2}{W_1} * 100 \tag{1}$$

where VC is the volatile matter content, W_1 is the initial weight of sample, W_2 is the final weight of sample.

$$FC\ (wt.\ \%) = 100 - (MC + AC + VC) \tag{2}$$

where FC is the fixed carbon content, MC is the total moisture content, AC is the total ash content, and VM is the volatile matter content.

Morphological and chemical composition analysis

A scanning electron microscope (SEM) (JSM-IT100, Jeol Ltd., Tokyo, Japan) coupled with an energy dispersive X-ray spectrometer (EDS) (XFlash Detector 410-M, Bruker Nano GmbH, Berlin, Germany) was used to analyse the surface morphology and chemical composition of the meal and biochar samples. The EDS was applied to analyse the weight% concentrations of some of the most important elements including sodium (Na), potassium (K), calcium (Ca), magnesium (Mg), aluminium (Al), iron (Fe), silicon (Si), phosphorous (P), carbon (C), sulphur (S), and oxygen (O). Furthermore, based on the chemical composition, the O/C atomic ratio was calculated using Eq. 3.

$$\frac{O}{C} = \frac{\%Oxygen/Atomic\ weight\ of\ oxygen}{\%Carbon/Atomic\ weight\ of\ carbon} \tag{3}$$

Less than 0.01 g of a sample was first coated with a thin carbon film and an alloy of gold and palladium (80% Au and 20% Pd), and its surface was kept electrically conductive to prevent image distortions in a Sputter coater (SCD 050, BAL-TEC). Three different magnifications (100×, 50×, and 10×) utilized for each of the samples. The analysis was performed at the Materials Engineering Department, University of Applied Sciences (HTW) Berlin, Germany.

Mercury intrusion porosimetry (MIP) characterization

The MIP was used to analyze properties such as bulk density (g mL^{-1}), skeletal density (g mL^{-1}), bulk volume (mL g^{-1}), skeletal (pore) volume (mL g^{-1}), pore diameter (μm), pore diameter distribution, porosity (%), total intrusion volume (mL g^{-1}), and total pore area (m^2 g^{-1}). The analysis was performed at the Federal Institute for Materials Research and Testing (BAM), Berlin, Germany, by the Department of Structural Analysis, employing a Mercury Porosimeter (Autopore V 9600, Micromeritics, USA).

Specific surface area analysis

The BET method for determining the specific surface area of solids by gas adsorption is a standard procedure detailed in ISO 9277[64]. This approach necessitates pre-conditioning the samples in helium or nitrogen flow at a specific temperature, referred to as outgassing, to reduce interferences in measurements caused by gases and vapors that can be physically adsorbed on the surface of the particles. Outgassing is one of the main causes of variation in the findings obtained using this approach[42]. This outgassing method is used to remove all adsorbed gases and water from a sample using a combination of vacuum, heat, and inert gas purging for a specific sample weight.

The specific surface areas of the meal and char samples were studied using dynamic vapor sorption (DVS) method which employs water vapor, krypton gas and nitrogen gas adsorption techniques. The first two analytical procedures were carried out at the Federal Institute for Materials Research and Testing (BAM) in Berlin, Germany, by the Department of Structural Analysis. In contrast, the last procedure was performed at the German Biomass Research Centre (DBFZ) located in Leipzig, Germany. In preparation for the analysis, the meal and char samples were subjected to the requisite conditioning. Consistent with the established methodology outlined by[43], the process necessitated outgassing the samples to fully remove surface-adsorbed gases, moisture, and any extraneous materials. Below are the details of the approaches.

Dynamic vapor sorption (DVS) analysis. The DVS approach is an analytical technique that measures the adsorption of water (or another solvent) onto powdered particles as a function of relative humidity (or the partial pressure of the solvent) at a fixed temperature[44]. The analysis was executed utilizing a DVS RESOLUTION device from Surface Measurement Systems Ltd. (SMS) at room temperature (298K).

Nitrogen gas (N_2) adsorption. The specific surface area (S_{BET}) analysis, employing nitrogen sorption, was conducted utilizing an automated gas sorption analyser (Autosorb iQ, Quantachrome Instruments, USA). The

analytical system features turbomolecular vacuum pumps and was operated under cryogenic conditions at 77 K. Sample masses of 0.43 g (Yellow Dodolla biochar) and 0.64 g (Holetta-1 biochar) were employed for the analysis. The subsequent outgassing was conducted at a final temperature of 523 K over a period of 12.8 h.

Krypton gas (Kr) adsorption. The specific surface areas (SSA) of the samples were determined by applying the Brunauer-Emmett-Teller (BET) adsorption isotherm model to data acquired via the krypton sorption method. The measurements were conducted utilizing an ASAP 2020 analyser (Micromeritics Instrument Corp.), an instrument equipped with turbomolecular vacuum systems and operated at a temperature of 77 K. The quantity of Kr gas adsorbed at relative pressures between 0.00 and 0.50 was used to determine the BET specific surface areas where the BET isotherms were linear and concave for meal and biochar samples, respectively.

Before adsorption measurements, the meal samples, Yellow Dodolla (3.21 g) and Holetta-1 (2.95 g) were degassed under vacuum at room temperature (295 K) for 24 h, and 4.5 days, respectively. To determine whether treatment at higher temperatures may produce better results, the first sample (2.34 g) was also analyzed at 423 K for 16 h. Similarly, before the adsorption measurements, Yellow Dodolla biochar was degassed under vacuum at two different temperatures: room temperature (295 K) for 2 days and 423 K for 16 h. The weights of the samples were 1.75 and 1.11 g, respectively.

Results

Proximate analysis

According to the results of the proximate analysis conducted on the *B. carinata* biochars, indicated in wt%, the Yellow Dodolla displayed a total moisture content of 5.14, a total ash content of 14.80, a volatile matter content of 26.27, and a fixed carbon content of 53.79. However, the Holetta-1 showed a total moisture content of 4.19, total ash content of 10.93, volatile matter content of 41.15, and fixed carbon content of 43.73.

Morphological characterization

In this section, the SEM-EDS results of the meal and biochar samples is presented, with Figs. 1 and 2 illustrating the significant morphological transformations that occurred during the thermochemical conversion process[41].

Nutrient profile analysis

The results, which are shown below in wt% for both the Holetta-1 and Yellow Dodolla samples, indicate the nutrient profile of the biochars. K (1.49), Ca (0.76), Mg (0.36), Fe (0.11), and P (0.48) were the main elements present for the Yellow Dodolla biochar. In the same way, the concentrations of K (1.32), Ca (0.78), Mg (0.39), Fe (0.02), and P (0.64) were observed in the Holetta-1 compost. There was no detectable amount of silicon (Si), aluminium (Al), or sodium (Na) in either biochar.

Ultimate composition analysis

The results of the ultimate analysis confirmed that the Yellow Dodolla biochar possessed 86.64 wt.% carbon (C), 0.39 wt.% sulfur (S), and 9.77 wt.% oxygen (O). Holetta-1 biochar, on the other hand, had a slightly varied composition, having percentages of C, S, and O of 86.33 wt.%, 0.10 wt.%, and 10.41 wt.%, respectively. The

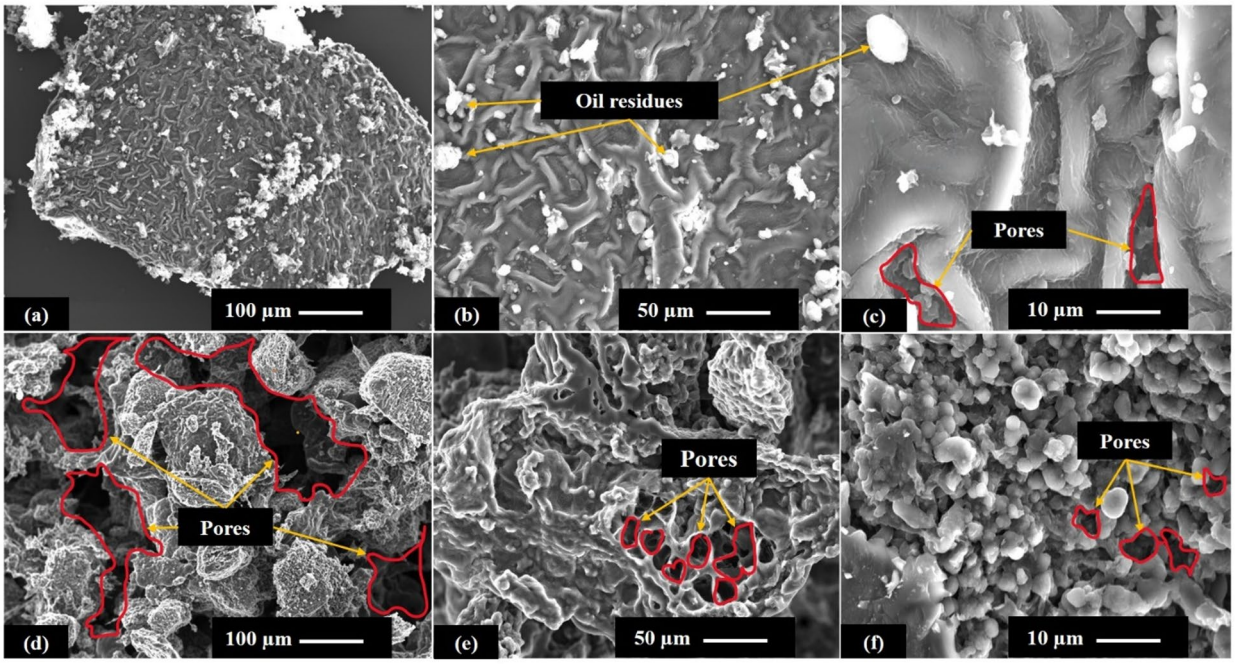

Fig. 1. Scanning electron microscope images of Yellow Dodolla. (**a**) and (**c**) meal; and (**d**) and (**f**) biochar at three different magnifications.

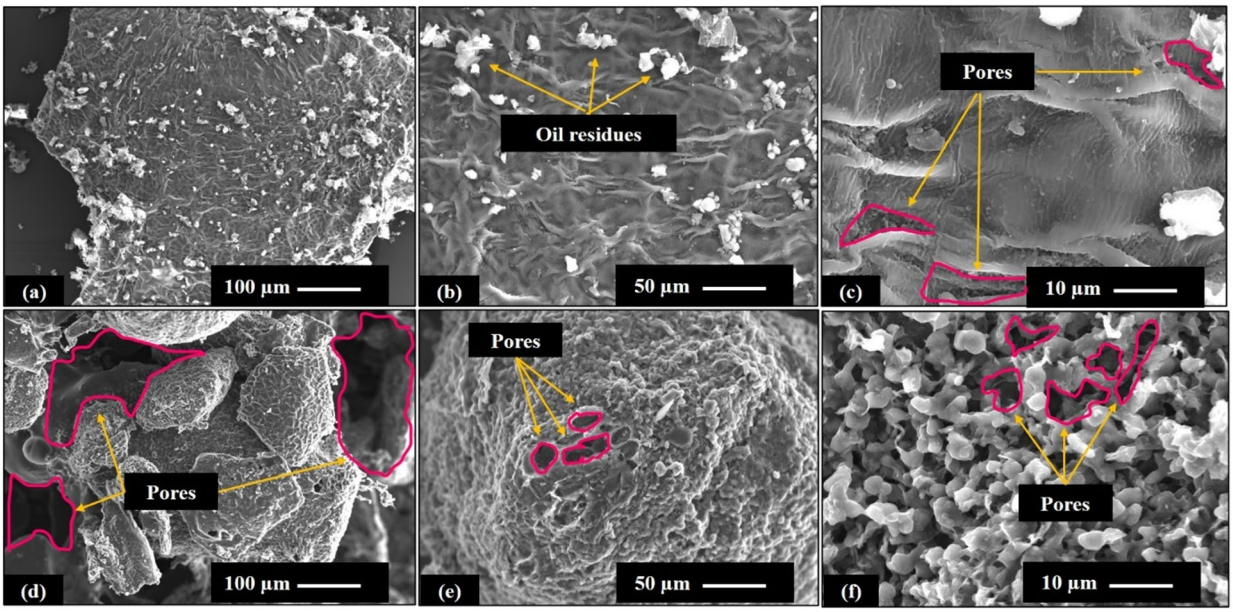

Fig. 2. Scanning electron microscope images of Holetta-1. (**a**) and (**c**) meal; and (**d**) and (**f**) biochar at three different magnifications.

Property	Yellow Dodolla		Holetta-1	
	Meal	Biochar	Meal	Biochar
Bulk density (g mL^{-1})	0.47	0.50	0.50	0.42
Apparent (skeletal) density (g mL^{-1})	1.22	1.35	1.24	1.42
Bulk volume (mL g^{-1})	2.11	1.99	2.14	2.36
Skeletal (pore) volume (mL g^{-1})	1.29	1.25	1.21	1.65
Pore diameter (µm)	13–410	18–411[a], 3.5–6.7[b]	9–410	10–411[c], 3–6[d]
Porosity (%)	61.01	62.68	59.93	69.99
Total intrusion volume (mL g^{-1})	1.29	1.25	1.21	1.65
Total pore area (m^2 g^{-1})	9.35	(-)	12.64	(-)
Median pore diameter (volume) (nm)	62,794.52	(-)	49,753.87	(-)
Median pore diameter (area) (nm)	7.24	(-)	5.92	(-)

Table 1. Mercury intrusion porosimetry characterization of *B. carinata* Biochar and meal.

presented results indicate that both materials are highly rich in carbon, with oxygen ranking as the second most prominent element. Sulfur appears in very small quantities.

18–411[a] and 10–411[c]: represent log differential pore size distribution (PSD). 3.5–6.7[b] and 3–6[d]: represent the cumulative pore size distribution (PSD). (-): represent that the data is not available. Meal: raw *B. carinata* (biomass) feedstock. Biochar: pyrolyzed product. Yellow Dodolla: A type of *B. carinata* cultivar. Holetta-1: A type of *B. carinata* cultivar.

Mercury intrusion porosimetry characterization

Table 1 was generated using the intrusion data, which is displayed in Supplementary Tables S1–S7 and Tables S8–S15, respectively, for biochar and meal samples. This table offers an in-depth summary of the main findings from the meal and biochar samples' MIP analysis. The study's subsequent sections went into greater depth about this table.

Specific surface area analysis

Dynamic vapor sorption

Given that the DVS results were found to be unreliable for precisely describing the surface area of the meal and biochar samples, they are not included in this section. A thorough explanation of this finding is offered in the Discussion section of the study.

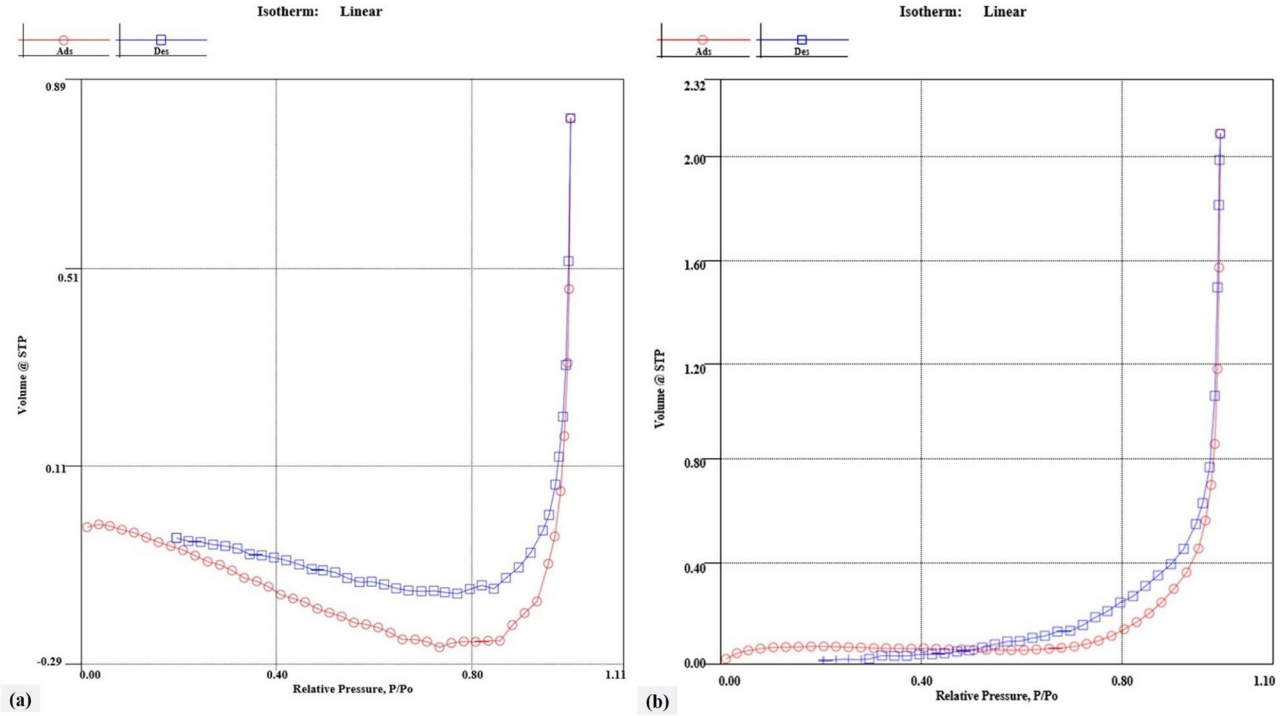

Fig. 3. Nitrogen adsorption-desorption isotherms for (**a**) Yellow Dodolla and (**b**) Holetta-1 biochars.

Sample Type	Preparation Conditions	SSA ($m^2\ g^{-1}$)	Relative Pressure* (p/p_0)	C-Value	Correlation Coefficient
Yellow Dodolla	2 days at RT	0.15	0.05 – 0.21	19.19	0.9999743
	16 h at 423 K	0.17	0.05 – 0.21	34.62	0.9999697
Holetta-1	2.5 days at RT	0.23	0.05 – 0.21	17.37	0.9999803
	16 h at 423 K	0.26	0.05 – 0.21	33.98	0.9999762

Table 2. Krypton adsorption specific surface area of biochars under varying Preparation conditions. RT: room temperature. SSA: specific surface area. *: shows the calculated relative pressure. Yellow Dodolla: A type of *B. carinata* cultivar. Holetta-1: A type of *B. carinata* cultivar.

Nitrogen gas adsorption
Figure 3 shows the nitrogen adsorption-desorption isotherms that are utilized to characterize the Holetta-1 and Yellow Dodolla biochars.

Krypton gas adsorption
Table 2 was generated using the Kr gas adsorption data, which is shown in Supplementary Tables S16–S19 and Tables S20–S22, respectively, for biochar and meal samples.

Discussion

Proximate nalysis of *B. carinata* Biochar

Table 3 presents the proximate analysis of biochar generated from Yellow Dodolla and Holeta-1. The analysis offers a robust profile of the biochar's total moisture content, total ash content. volatile matter, and fixed carbon. The experimental results showed a fixed carbon content of 54–44 wt.%, indicating an exceptionally stable product showing an outstanding carbon sequestration opportunity. Given its substantial fixed carbon level and relatively small volatile matter content of 26–41 wt.%, the biochar likely originated, at optimal pyrolysis environments at a temperature that would have devolatilized the majority of organic molecules, as reported in[41], while maintaining the carbon-rich matrix. A significant factor influencing the practicability of the biochar for establishing a sustainable agriculture (i.e., as soil supplement) is its ash content (Table 3).

A comparison of the current investigation's findings to those presented in the existing literature (Table 3) demonstrates a strong agreement with accepted criteria for biochar generated from similar agricultural materials. The present study's fixed carbon content, specifically that of Yellow Dodolla, is considerably lower compared to that of the biochar made from Wheat Straw Biochar [45] yet substantially greater than that of the biochar made from Peanut Shell Biochar[46]. Additionally, it was found that the samples had a higher ash content than what

Property	Experimental Value (wt.%)		Literature Value (wt.%)		
	Yellow Dodolla Biochar	Holeta-1 Biochar	Wheat Straw Biochar[45]	Peanut Shells Biochar[46]	Rapeseed Biochar[48]
Total moisture	5.14	4.19	0.6 ± 0.01	5.44	6.30[47]
Total ash	14.80	10.93	8.2 ± 0.2	3.8	19.28
Volatile matter	26.27	41.15	7.3	56.6	25.14
Fixed carbon	53.79	43.73	83.9	34.06	55.58

Table 3. Proximate analysis of *B. carinata* Biochar compared to previously reported values. Biochar: pyrolyzed product. Yellow Dodolla: A type of *B. carinata* cultivar. Holetta-1: A type of *B. carinata* cultivar. 6.30[47] : Rapeseed stem derived biochar.

Table 3 stated for the Wheat Straw and Peanut Shell biomass. This shows that *B. carinata* biochar could be a useful source of plant-available nutrients when applied to soil.

Furthermore, the Yellow Dodolla and Holetta-1 biochars were compared with biochars derived from rapeseed meal and rapeseed stem (Table 3). The total moisture content of these experimental biochars is identical to that reported for biochar derived from rapeseed stem (6.30 wt.%)[47]. While the total ash content of these biochars was observed to be slightly lower than that of the rapeseed biochar (19.28 wt.%)[48], the volatile matter content of Holetta-1 is substantially higher than this reported value. Yellow Dodolla's volatile matter content, however, is similar to this reported value. Furthermore, although the fixed carbon content of Holetta-1 is slightly lower than this value, the fixed carbon content of Yellow Dodolla is identical to the reported value. In general, the harmony of these observed qualities with values reported in the literature highlights the potential of *B. carinata* biochar as a useful and efficient raw material for energy, environmental, and other commercial uses.

Morphological characterization

Figures 1 and 2 show the surface morphologies of the meal and biochar samples. At higher magnifications, as shown in Figs. 1 (b) and (c), and 2 (b) and (c), rod-like structures, most likely fibers, and some white spots were observed. The observed spots are likely residual miscella (oil and solvent) retained within the meal following the solid-liquid separation (filtration) stage of solvent extraction. All of the white color spots may not represent oil residue, though, as the samples also get charged during SEM analysis. Due to the possibility that the fibers were decomposed and the oil residues were burned off during the pyrolysis experiment while the biochars were produced, the fibers are not evident in the biochar samples, as evidenced in Figs. 1 (d) to (f), and 2 (d) to (f).

The analysis revealed heterogeneous pores of varied sizes and shapes. This observation is further substantiated by a prior study[49], which describes the volatilization of organic matter and subsequent pore development as a consequence of thermalization. Similarly, the decomposition of organic matter during pyrolysis enhanced porosity, which led to the formation of channels and pores on the surface of biochars[49]. The morphological characteristics, as shown in Figs. 1 and 2, are essential for understanding the material's efficacy in various industrial applications. Crucially, the presence of extensive pore network of the biochar samples likely contributes directly to the overall specific surface area, which typically acts as the primary parameter governing the biochar's capacity for adsorption applications.

Nutrient profile analysis

Table 4 shows the EDS chemical composition analysis (atomic percentages) of the biochar samples, with the results confirming that sodium, aluminium, and silicon were not detected. The concentrations of the remaining metals, with potassium concentration being the highest, were observed to increase when compared to their reported pre-pyrolysis values[40]. In general, the thorough analysis of the experimental findings show that the type of feedstock did not significantly affect the elemental concentrations.

The use of organic amendments like compost and other organic waste materials boosts the bio-availability of key nutrients such as nitrogen (31 wt.%), phosphorus (25 wt.%), and potassium (23 wt.%) when compared with commercial fertilizers, while also conditioning the soil[50]. Given that chemical fertilizers are often expensive due to production costs[51], the organic fertilizers derived from biomass—such as the biochar in the present investigation, which has an ample potassium content of 1.49 wt.% and 1.32 wt.% for Yellow Dodolla and for Holetta-1, respectively—can be applied as viable alternative amendments for sustainable agriculture.

To facilitate comparisons against the findings of the experiment, Table 4 also provides reported values for biochar derived from Wheat Straw, Timothy Grass, and Sugarcane Filter. The majority of the nutrients in the biochar had concentrations that are comparatively greater than the reported results stated in Table 4. Additionally, Table 4 shows a large variation in the concentrations of other important elements. The experimental biochar contains significantly higher P concentrations than Timothy grass biochar and Wheat straw biochar, indicating a potential benefit for agricultural uses that require P supplement. Furthermore,

On the other hand, the experimental samples' Fe content is significantly lower than the value reported in the available literature for sugarcane filter biochar Table 4. It is expected, therefore, that most of the elements are concentrated in the biochars rather than the bio-oil during the oilseed meals pyrolysis experiment[41]. The absence of these elements renders the bio-oil a valuable substitute feedstock for upgrading through catalytic reactions. On the other hand, these components' existence in the biochars is advantageous for a variety of industrial uses.

The measured concentrations of the three main elements—C, S, and O—in the ultimate composition investigation are displayed in Table 4. In comparison to the oilseed meals[40], the biochar samples had significantly reduced S and O levels. In contrast, the C content of the biochar (ca. 86 wt.%) (Table 4) is much greater than that

Type of Analysis	Experimental Value (wt.%)		Literature Value (wt.%)		
	Yellow Dodolla Biochar	Holetta-1 Biochar	Sugarcane Filter Biochar[49]	Timothy Grass Biochar[45]	Wheat Straw Biochar[45]
Nutrient					
Na	ND	ND	0.010	0.001	0.002
K	1.49	1.32	(-)	0.008	0.008
Ca	0.76	0.78	0.68	0.001	0.031
Mg	0.36	0.39	0.21	0.000	0.003
Al	ND	ND	(-)	0.027	0.000
Fe	0.11	0.02	1.34	0.067	0.002
Si	ND	ND	(-)	(-)	(-)
P	0.48	0.64	1.297	0.000	0.002
Ultimate					
C	86.64	86.33	81.35 ± 1.42[52]	45.15 ± 0.33[53]	64.8
S	0.39	0.10	(-)	0.04	0.1
O	9.77	10.41	15.23 ± 1.27[52]	7.12 ± 0.16[53]	23.0
O/C	0.08	0.09	0.14 ± 0.015[52]	0.12[53]	0.3

Table 4. Nutrient and ultimate composition of *B. carinata* Biochar compared to literature values.

of its pre-pyrolysis *B. carinata* oilseed meal (ca. 51 wt.%), as reported in[40], indicating that the thermochemical conversion process significantly raised the C content. These ultimate composition results were compared to existing literature values, as shown in Table 4, and it emerged that the biochar samples from Yellow Dodolla (86.64 wt.%) and Holetta-1 (86.33 wt.%) had notably elevated C contents. This stands in contrast to the reduced C percentage recorded for Timothy grass biochar (45.15 ± 0.33 wt.%) and Wheat straw biochar (64.8 wt.%).

Na: sodium. K: potassium. Ca: calcium. Mg: magnesium. Al: aluminium. Fe: iron. Si: silicon. P: phosphorous. C: carbon. S: sulphur. O: oxygen. O/C: oxygen to carbon atomic ratio. (-): represent that the data is not available. ND: Not detected. Biochar: pyrolyzed product. Yellow Dodolla: A type of *B. carinata* cultivar. Holetta-1: A type of *B. carinata* cultivar.

Ultimate composition analysis

The O/C ratios of the biochars are shown in Table 4, with the results showing that they are significantly lower than the reported values for Sugarcane filter biochar, Wheat straw biochar and Timothy grass biochars (Table 4). As reported in[54], metal ions and contaminants can be bound to the surface of biochar by oxygen-containing functional groups. Furthermore, the level of aromaticity and polarity of biochars were frequently associated with their O/C atomic ratios. Both the Yellow Dodolla and Holetta-1 biochars have reduced O/C ratios (Table 4) than their respective meal feedstocks[40], reflecting a greater degree of carbonization. Additionally, the O/C ratios of these two biochars were nearly comparable, indicating that their thermal breakdown paths and ultimate product properties were similar under the pyrolysis environment.

The O/C atomic ratios of the experimental samples (Table 4) is further supported by the prior study[55], which indicated that when the pyrolysis temperature rises, more O and H, as well as organic molecules, tar, and surface components, are released, resulting in a drop in the H/C and O/C ratios in the final biochar. According to the literature, biochars with an O/C ratio < 0.2 are very stable, biochars with an O/C ratio between 0.2 and 0.6 are moderately stable, and biochars with an O/C ratio greater than 0.6 are rather unstable[55]. As a result, because the current samples' O/C ratios are substantially lower than the reported value (i.e., 0.2), they are very stable and can be used for agricultural and environmental remediation.

Mercury intrusion porosimetry characterization

Intra-particle porosity analysis

Table 5 presents the findings of the evaluation of parameters including bulk density, skeletal density, bulk volume, skeletal (pore) volume, pore diameter, pore diameter distribution, and porosity using mercury intrusion porosimetry. The biochar samples, particularly Holetta-1, show a bit higher total intrusion pore volume than its respective meal. The samples with the highest porosity are those with Holetta-1 biochar, and this enhanced porosity may be related to the biochar's slightly bigger bulk, and skeletal (pore) volumes (Table 5). The porosity of Yellow Dodolla increased little after pyrolysis, but that of Holetta-1 increased by roughly 10 wt%.

Figure 4 illustrates the mercury intrusion-extrusion cycles as a function of pressure for both the intrusion and extrusion of mercury. As seen in this figure, the intrusion of mercury into the oilseed meals differs slightly from that of the biochars in that the particles are compressed at the onset of the intrusion in the meals, as indicated by B and E in Fig. 4 (a) and (c), but this is not noticed in the biochar samples. The intrusion-extrusion of a cycle in the oilseed meals is also distinct from that in biochar samples because, even if the loop is open, the cycle of the meals appears to be closing, whereas this is not the case with the biochar samples. Since a mercury molecule may have been entrained during extrusion in both situations, the open loops might have developed as a result.

Mercury intrusion curves, as depicted in Fig. 4, have been developed to demonstrate the correlation between mercury pressure and cumulative intrusion. As the pressure got higher, the results showed that mercury molecules

Property	Yellow Dodolla		Holetta-1	
	Meal	Biochar	Meal	Biochar
Bulk density (g mL^{-1})	0.47	0.50	0.50	0.42
Apparent (skeletal) density (g mL^{-1})	1.22	1.35	1.24	1.42
Bulk volume (mL g^{-1})	2.11	1.99	2.14	2.36
Skeletal (pore) volume (mL g^{-1})	1.29	1.25	1.21	1.65
Pore diameter (μm)	13–410	18–411[a], 3.5–6.7[b]	9–410	10–411[c], 3–6[d]
Porosity (%)	61.01	62.68	59.93	69.99
Total intrusion volume (mL g^{-1})	1.29	1.25	1.21	1.65
Total pore area (m^2 g^{-1})	9.35	(-)	12.64	(-)
Median pore diameter (volume) (nm)	62,794.52	(-)	49,753.87	(-)
Median pore diameter (area) (nm)	7.24	(-)	5.92	(-)

Table 5. Mercury intrusion porosimetry characterization of *B. carinata* Biochar and meal. 18–411[a] and 10–411[c]: represent log differential pore size distribution (PSD). 3.5–6.7[b] and 3–6[d]: represent the cumulative pore size distribution (PSD). (-): represent that the data is not available. Meal: raw *B. carinata* (biomass) feedstock. Biochar: pyrolyzed product. Yellow Dodolla: A type of *B. carinata* cultivar. Holetta-1: A type of *B. carinata* cultivar.

intruded even the smallest pores in the oilseed meal and biochar samples, revealing insights pertaining to the materials' porosity and pore size distribution. The intrusion of mercury molecules increases significantly as the intrusion pressure rises until it basically approaches equilibrium at 10 MPa for the meals (Fig. 4, (a), and (b)); however, after 10 MPa, intrusion becomes almost constant. Conversely, this is not the case with the biochars, where intrusion keeps very slowly rising even after 10 MPa. Figure 4 (b) shows that Holetta-1 biochar was found to have a higher intrusion of mercury molecules than the other samples, indicating that it is more porous. This is perfectly consistent with the measured Holetta-1 porosity presented in Table 5.

The bulk density of the meal and biochar samples is slightly bigger than the reported values of the biochar produced from sugarcane filters (0.131 g cm^{-3}). However, compared to the porosity of the biochar from the sugarcane filters (76.56%)[49], the samples' porosity, particularly that of the Yellow Dodolla, is relatively lower. Additionally, there exists no apparent distinction in the porosity of Yellow Dodolla meal and its biochar. This could imply that volatile constituents may have been remained in the Yellow Dodolla biochar even following the pyrolysis experiment. The bulk density of the samples is another feature; it ranges from 0.42 to 0.50 g mL^{-1}, which is consistent with the results of 0.09 to 0.5 g cm^{-3} reported in[49]. In addition, the samples had a substantially larger total incursion pore volume than corncob-derived biochar (0.0405 ± 0.0041 cm^3 g^{-1})[52].

Pore size distribution

Table 5 shows the pore size distributions (PSD) estimated via log differential intrusion and cumulative intrusion. Also, the PSD is displayed in Fig. 6 where the representative pores from the SEM images in Figs. 1 and 2 can be considered. The log differential PSD is used to characterize the skeletal and bulk volumes, skeletal and bulk densities, and porosities shown in Table 5 where the distribution of pores was varied from 13 to 410 μm and 18 to 411 μm for Yellow Dodolla oilseed meal and biochar, respectively. For meals and biochar of Yellow Dodolla, the most frequent pore sizes are 124.37 μm and 172.46 μm, respectively.

Based on these observations and the data provided in Table 5, the Yellow Dodolla oilseed meal has lower bulk and skeletal densities, as well as porosity, than its biochar; nonetheless, the meals' bulk and skeletal volumes are slightly lower than the biochar. In both types of samples, the porous and non-porous components of the log differential pore size distributions displayed in red (Fig. 6) exhibit sharp and long peaks showing the inter-particle volumes, and those indicated by circles represent the real pores. Furthermore, cumulative pore size distributions are varied from 3.5 to 6.7 μm for the biochar.

Similarly, the skeletal and bulk volumes, skeletal and bulk densities, and porosities of Holetta-1 depicted in Table 5 are characterized utilizing the log differential PSD, where the distribution of pores was increased from 9 to 410 μm and 10 to 411 μm, respectively, for the meal and its biochar. The most frequently occurred pore sizes are 79.93 μm and 111.42 μm, respectively, for the meal and its biochar. However, except for the bulk density, other parameters including the skeletal density, the bulk and skeletal volume, as well as the porosity of this biochar are greater than that of its meal. It becomes apparent that Holetta-1 biochar is more porous than Yellow Dodolla biochar.

Inter-particle porosity analysis

The effect of biochar on soil's hydraulic characteristics and aeration is dependent on the size, shape, and quantity of the pores between soil particles as well as the inter- and intra-particle pores in the biochar[56]. Alternatively, it might be explained by the fact that biochar possesses pores inside of its particles (intra-pores), which may offer more space to hold water storage in addition to the pores between its particles (inter-pores)[56].

As a result, since the meals do not have true porous structures, inter-particle porosity was utilized to determine characteristics including skeletal volume, pore diameter distribution, and porosity, the results of which are presented in Table 6. Table 6 further shows the values of the biochars in addition to the results of the

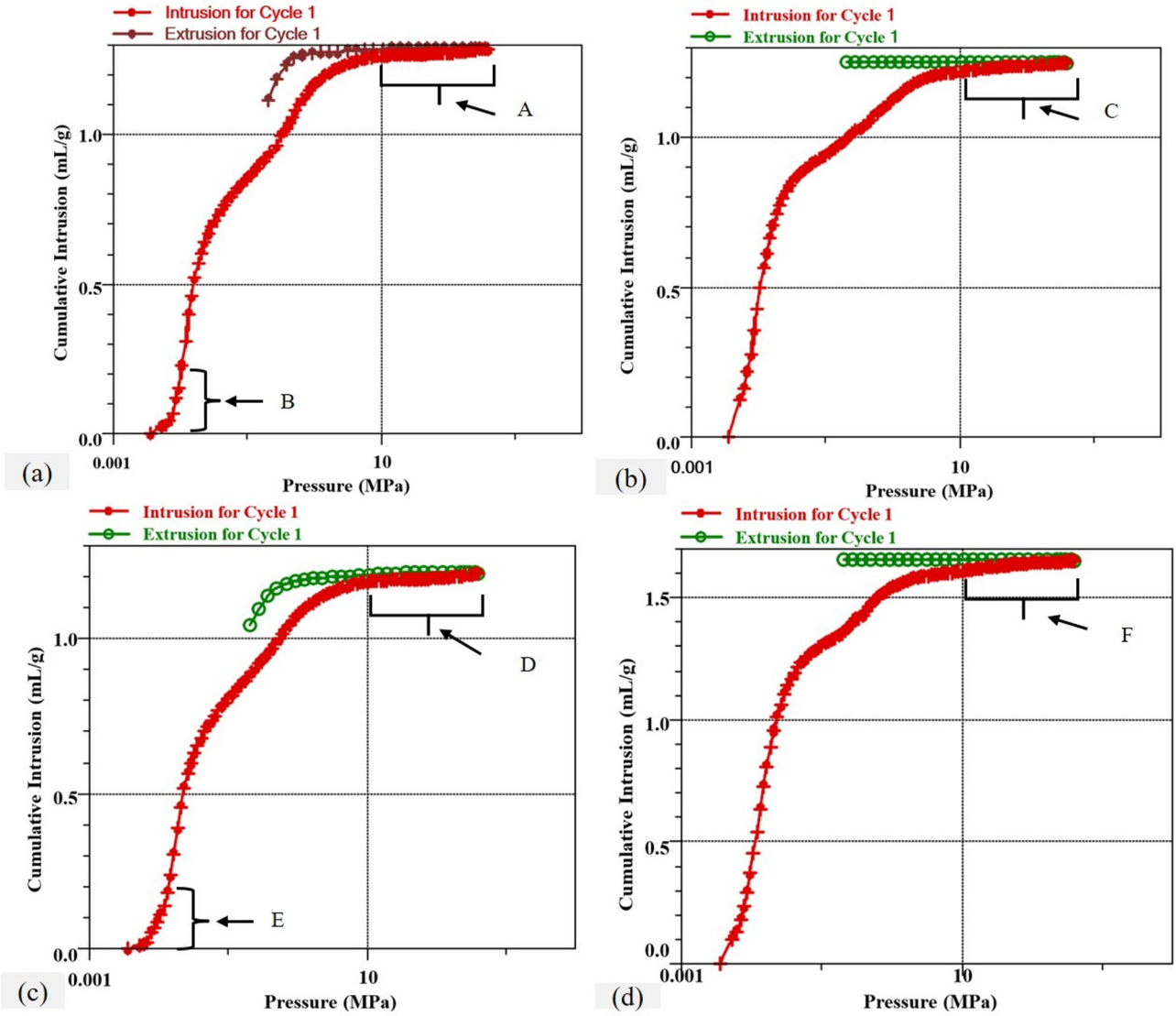

Fig. 4. Mercury intrusion-extrusion profiles for: (**a**) Yellow Dodolla meal, (**b**) Yellow Dodolla biochar, (**c**) Holetta-1 meal, and (**d**) Holetta-1 biochar.

Property	Yellow Dodolla		Holetta-1	
	Meal	Biochar	Meal	Biochar
Skeletal volume (mL g^{-1})	0.43	0.32	0.37	0.33
Pore diameter (nm)	3.10–14, 814.60	3.59–18, 696.39	3.59–1, 019.63	3.59–11, 693.55
Porosity (%)	20.49	16.05	17.39	13.92

Table 6. Porosity and pore diameter distribution of *B. carinata* Biochar and meal. Yellow Dodolla: A type of *B. carinata* cultivar. Holetta-1: A type of *B. carinata* cultivar. Meal: raw *B. carinata* (biomass) feedstock. Biochar: pyrolyzed product.

meals. The results of the Leica microscope (Fig. 5) show that these widely scattered particles are appropriate for inter-particle porosity investigation. Figure 6 also shows the morphological characteristics of the meals, which clearly show that various types of particles do not have true porous structures.

As shown in Table 6, pore diameter distribution characterizes both the meal and biochar samples, with the upper limits reaching 18, 696.39 nm, indicate the presence of a significant macroporous structure in the studied biochars. Given that the N_2 adsorption isotherms (Fig. 3), the details of which are discussed in the subsequent section, are Type III with negligible hysteresis, the calculated large pore diameters likely correspond to the void spaces between aggregated particles rather than well-defined internal pore channels. The bigger patterns

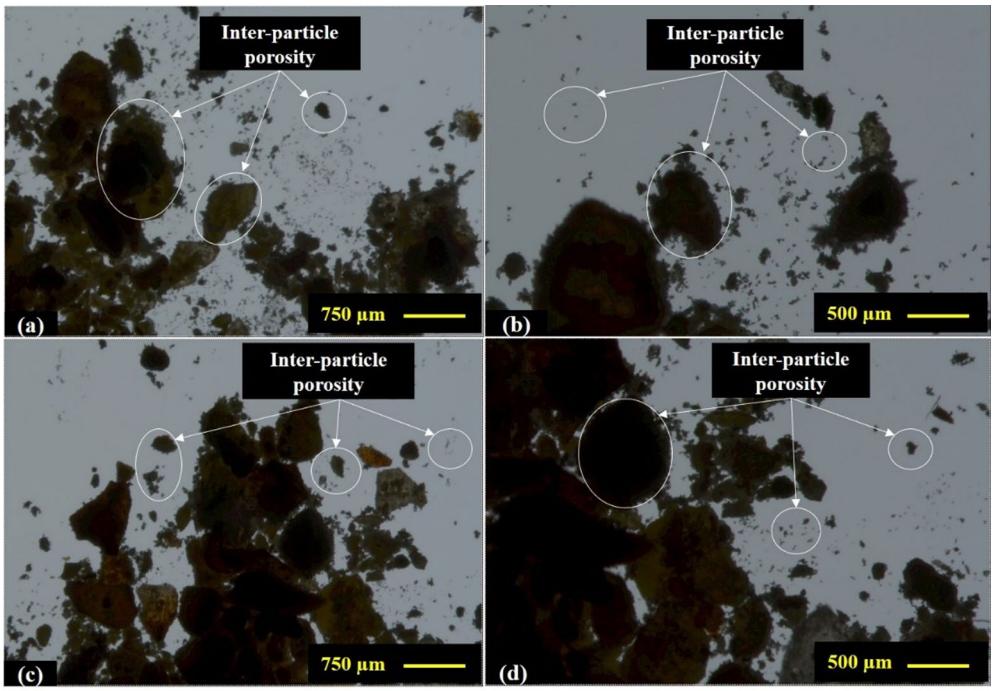

Fig. 5. Leica microscope images showing the inter-particle porosity of Yellow Dodolla (**a**) and (**b**), and Holetta-1 (**c**) and (**d**) meals at different magnifications.

could be attributable to the interparticle spaces or cavities within the biochar or meal particles, or they could be fundamental macro- channels and bigger structural characteristics found in the initial biomass.

The occurrence of "template-effect" or " intrinsic architecture retention" explains the analogy in pore structure (or particular structural properties) between the initial biomass meals and the produced biochars. The cell walls' organic elements could have been eliminated by the thermal breakdown, but the stiff, skeletal structure—which serves as a template—remains mostly unbroken.

The pore diameters of the samples are observed to be higher than the average pore diameter of a biochar obtaind from corncob (2.872 nm)[52]. The log and cumulative pore size distributions are used to describe the pore size distributions for the inter-particle porosities. The four samples (Table 6) all exhibit different pore size distributions, but in nearly all of them, the pore volume (ml g^{-1}) rises sharply when the pore size (nm) declines, and vice versa.

Specific surface area analysis

Specific surface area is one of the most vital features of biochar, with the type of feedstock being one of the primary factors[57] governing the release of volatile components and the subsequent development of pores[58]. Following examination using various gas adsorption techniques, the surface areas determined in the current investigation are detailed below and compared with reported values from previous studies.

Dynamic vapor sorption

The specific surface areas of *B. carinata* meals and biochars underwent the DVS method; however, the results were not satisfactory. This result, based on gravimetric studies using solvents such as water vapor, shows that the approach's suitability to these materials may be limited. The absence of promising results could be due to poor adsorption of the recommended solvent into the surface of the materials, a phenomenon that is an important feature in correct DVS measurement.

Additional investigation is required to determine the exact reason of the recorded low adsorption properties. Possible causes include surface heterogeneity, the samples' chemical make up, or structural characteristics that could prevent the solvent molecules from interacting with the materials' surface. Other techniques, including BET analysis with various probing gases (like argon or nitrogen), could be required to get precise and easily reproducible specific surface area results for these types of substances.

Nitrogen gas adsorption

Gas adsorption is an established method for evaluating the texture of a wide range of porous solids and fine powders[59,60]. Nitrogen sorption is frequently employed to measure the distribution of pore sizes and surface area with highly porous, non-swelling materials[61]. In the present study, the volumetric nitrogen adsorption method resulted in negative isotherms, suggesting that the amount of nitrogen adsorbed onto the sample surfaces was below the detection limits or was otherwise insufficient for a positive measurement. This finding is supported by

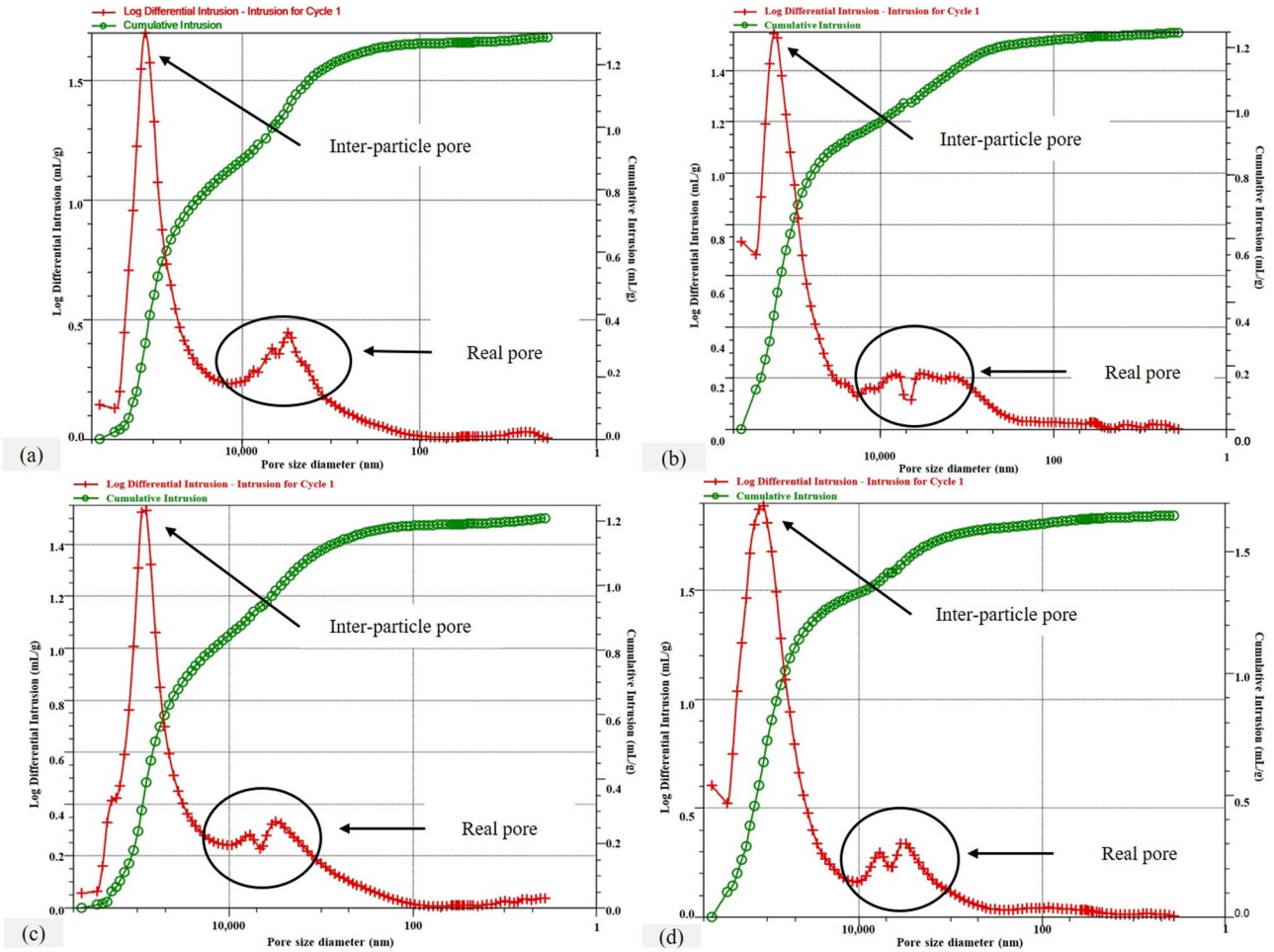

Fig. 6. Log differential intrusion and cumulative intrusion pore size distributions: (**a**) Yellow Dodolla meal and (**b**) its biochar; (**c**) Holetta-1 meal and (**d**) its biochar.

a prior report from[62], who concluded that nitrogen gas is unsuitable for the physisorption analysis of wood due to the high standard deviation observed in their BET measurements.

The N_2 adsorption-desorption isotherms presented in Fig. 3 (a) and (b) are characteristics of a Type III isotherm of Yellow Dodolla and Holetta-1 biochar samples, according to the International Union of Pure and Applied Chemistry (IUPAC) classification. In the figure, the labels "Ads" and "Des" indicate the adsorption and desorption curves, respectively. These isotherm shapes are defined by their convexity to the relative pressure (P/P_0) axis across the entire range, indicating that the adsorbate-adsorbent interactions (solid-gas) are weak compared to the adsorbate-adsorbate interactions (gas-gas). Due to the weak affinity of the adsorbent surface for the nitrogen gas, the formation of the first monolayer is thermodynamically unfavourable.

The type of isotherm observed in the samples develops as the relative saturation of the gas approaches unity and the amount of gas adsorbed rises without limit. The measured specific surface areas were determined to be 0.000 $m^2\ g^{-1}$ for Yellow Dodolla and 0.212 $m^2\ g^{-1}$ for Holetta-1, indicating a noticeable variation between the two samples. This observation may indicate that the Yellow Dodolla biochar possessed an insufficient surface area or exhibited an inability to adsorb nitrogen effectively. The second sample (Holetta-1) turned out to have a surface area, despite its exceptionally small size. In the section detailed below, these surface areas were also contrasted with those generated via krypton adsorption. In general, this methodology is deemed inappropriate for the surface area analysis of the present samples, primarily due to confounding factors such as nature of feedstock and the properties of the pore structure.

Krypton gas adsorption

Although N_2 (at 77 K) is the most frequently employed probe molecule for determining specific surface area, other adsorbates such as CO_2 (at 273 K), Ar (at 77–87 K), or Kr (at 77 K) can also be used, with each approach having its own benefits and drawbacks[63]. In the current study, it was confirmed that the DVS and nitrogen sorption were not efficient methods for estimating BET surface areas. However, Kr gas was successfully adsorbed at liquid nitrogen temperature (77 K), with Table 2 showing the Kr adsorption surface areas.

The S_{BET} of the samples was found to be < 1 $m^2\ g^{-1}$, which may be related to the study conducted on organic materials such as wood[62], in which krypton was found to be a more reliable adsorptive gas than nitrogen for

accurately detecting small surface areas. Despite the pyrolysis conditions (a temperature of 623 K, a heating rate of 10 K min^{-1}, and a holding time of 5 min), and feedstock type contributing to greater biochar yields[41], these same factors may have resulted in the low BET surface area.

The negligible BET uncertainties, as detailed in Table 2, confirm the precision of the estimated BET measurements. This, in turn, implies that krypton was the right adsorptive gas for the analysis in the current study. In a study conducted by[62], the nitrogen BET uncertainties were significantly larger than those for krypton, supporting our idea that krypton is preferable to nitrogen for small surface areas. The BET for Yellow Dodolla biochar at 423 K was found to have method measurement errors ranging from 7 to 10 which is the maximum among the others. However, there are no data available to make comparisons with the method measurement errors.

Because the surface areas were determined at higher pressures, it is possible that the samples began to devolatilize during preparation at 423 K. Lower temperatures may be preferable for preparation to prevent devolatilization, which could destroy the samples and prevent the analytical gas (Kr) from being properly adsorbed. Measurements indicated that Yellow Dodolla possessed a lower specific and total surface area than Holetta-1, regardless of whether the samples were dried at ambient temperature or 423 K. This is clearly observed in Figs. 1 (d) and 2 (d).

Figures 7 and 8 show the krypton adsorption isotherms of Yellow Dodolla and Holetta-1, respectively. The Kr adsorption isotherms for both sample types exhibit the characteristics of a Type II isotherm according to IUPAC classification. A key difference, however, is that the isotherms of the meal samples show a sharp increase as the relative pressure approaches unity, whereas the increase for the biochar samples is less pronounced. The rate of Kr adsorption in the biochar samples was higher than in the meals (Fig. 7 (c) and (d), with the biochar

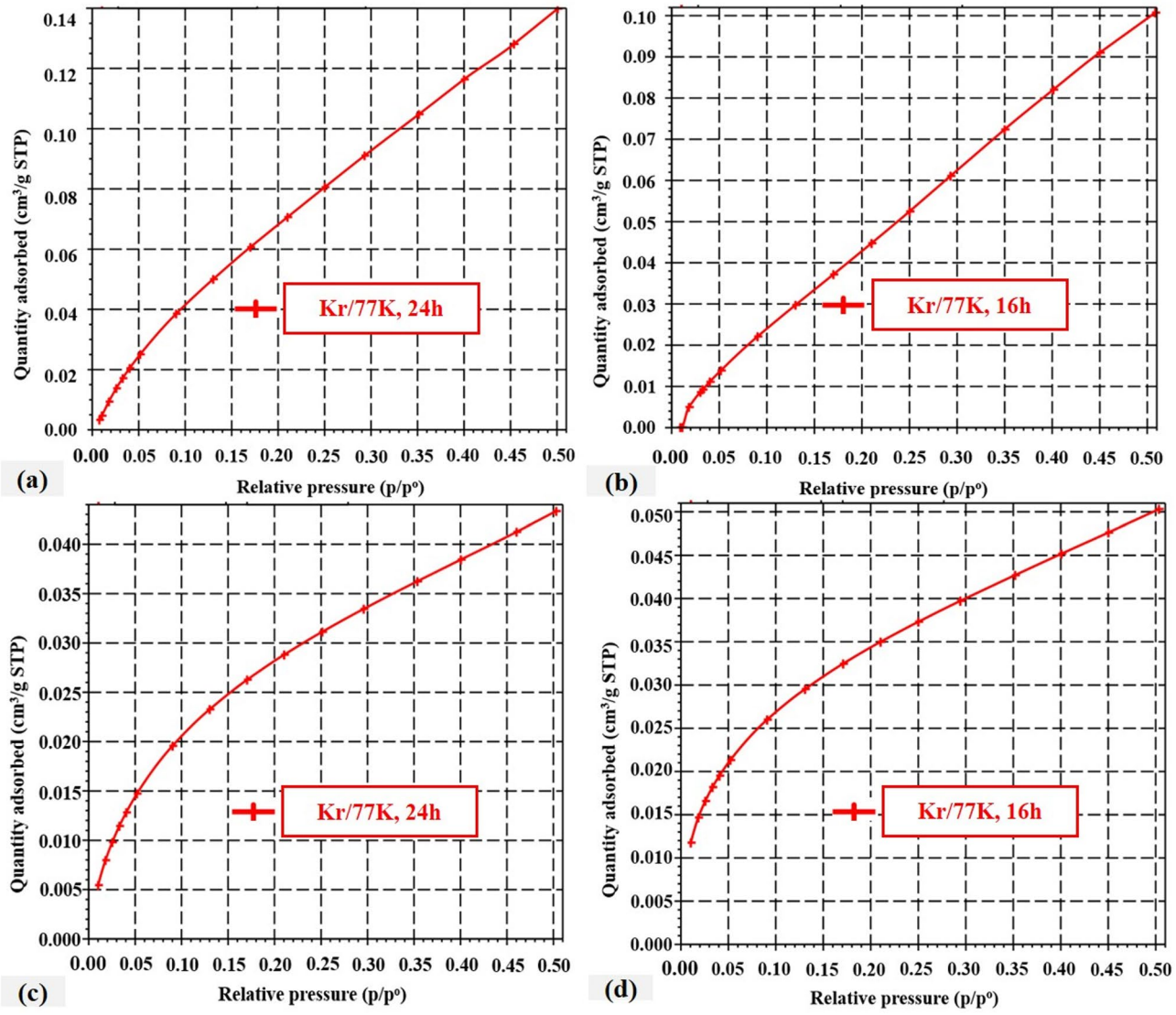

Fig. 7. Krypton physisorption isotherms measured at different temperatures for Yellow Dodolla **(a)** meal at room temperature, **(b)** meal at 423 K, **(c)** biochar at room temperature, and **(d)** biochar at 423 K.

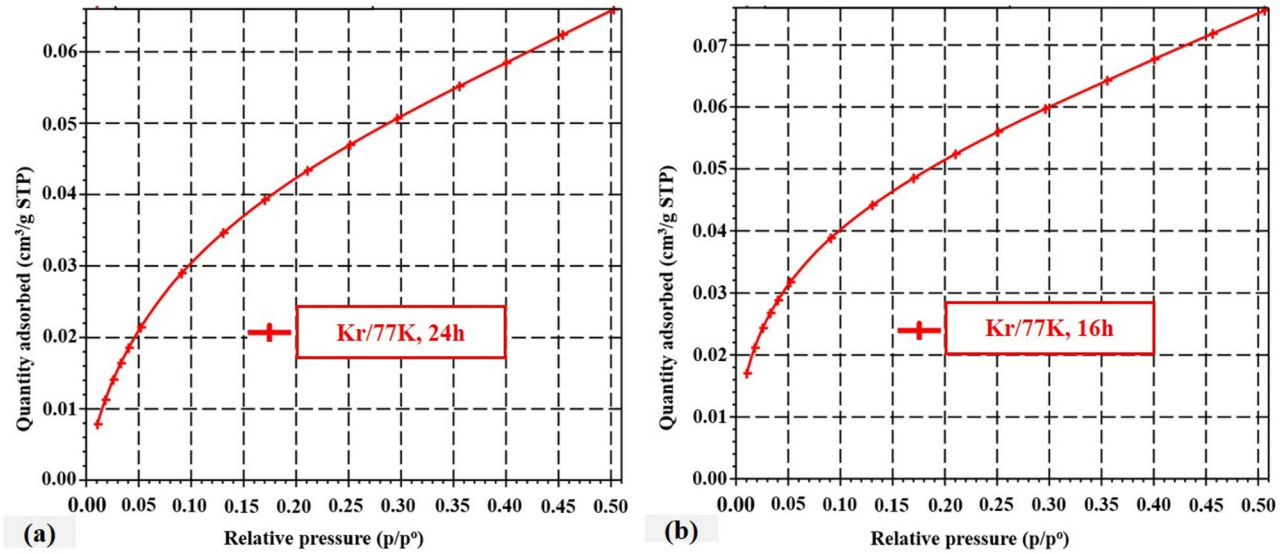

Fig. 8. Krypton physisorption isotherms for Holetta-1 biochar measured at various temperatures: **(a)** room temperature and **(b)** 423 K.

prepared at 423 K demonstrating the greatest adsorption capacity. Similar phenomena have been happened in the Holetta-1 samples where the highest amount of gas was adsorbed by the biochar sample (Fig. 8) compared to its pre-pyrolysis feedstock (i.e., the meal). In general, an initial high uptake was observed in the samples.

Potential industrial applications

Figure 9 schematically presents the *B. carinata* biochar synthesis, comprehensive physico-chemical characterization, and promising industrial applications. The characterisation qualities detailed previously indicate that the biochars generated from these species have a number of intriguing commercial uses. They constitute key materials for environmental remediation because of their affordable production costs, high carbon content, fundamental porous structure, and other exceptional characterization properties. Their structural porosity, for example, renders them suitable to be employed as adsorption materials in the purification of water and wastewater, where they may efficiently detoxify heavy metals, organic pollutants, and other impurities. As explained in the sections above, both Yellow Dodolla and Holetta-1 biochars contain notable levels of important macronutrients. The concentrations were determined to be K (1.49, 1.32), Ca (0.76, 0.78), and Mg (0.36, 0.39), respectively, all in wt.%.

This superior nutrient profile provides a more concentrated source of these key elements for plant growth. At 0.48 wt.% for Yellow Dodolla and 0.64 wt.% for Holetta-1, the P concentration is likewise comparatively high, underscoring its ability to improve soil fertility. Together with the macronutrients, the biochars have an excellent carbon content; for Yellow Dodolla and Holetta-1, the values are 86.64 wt.% and 86.33 wt.%, respectively. This is considerably greater than the majority of results reported in the scientific literature among different biochars, suggesting an exceptionally high level of stability and carbonization—two essential components for the retention of soil carbon over the course of time.

Because of their outstanding carbon content and a small atomic oxygen-to-carbon (O/C) ratio (0.08 and 0.09), such biochars appear to be very resistant and could stay within the soil for a prolonged period of time prior to degrading significantly. In general, their stability qualifies them for long-term use as soil amendments, where they could boost soil fertility, increase water retention, and store carbon, all of which support strategies to mitigate climate change and promote sustainable agriculture.

Notwithstanding their application in the environment, the biochars' unique qualities—most notably, their variety of pore sizes and shapes—indicate that they could be useful components in more targeted commercial procedures. The porosity, as demonstrated by methods including MIP, enables regulated interaction with gases and liquids. They are therefore outstanding options for gas storage and separation systems, in which particular gases, like carbon dioxide or hydrogen, can be tailored to be preferentially captured and stored. Moreover, their stability and high carbon content may be used for producing inexpensive electronic components for energy storage devices like batteries and supercapacitors, providing a sustainable substitute for traditional components.

In more general terms, the application of these biochars remains in line with the fundamental concepts of a sustainable and circular economic system. By turning agricultural waste products—like meals from *B. carinata*—into valuable raw materials, the approach reduces waste and generates additional income. These materials' effective characterisation highlights its promise as a flexible platform for a variety of commercial uses, ranging from advanced energy production and catalyst technologies to large-scale environmentally friendly options. In addition to providing financial advantages, this value-adding of agricultural waste materials supports sustainable use of resources, underscoring the important role these resources could serve in the shift to a less harmful industrial environment.

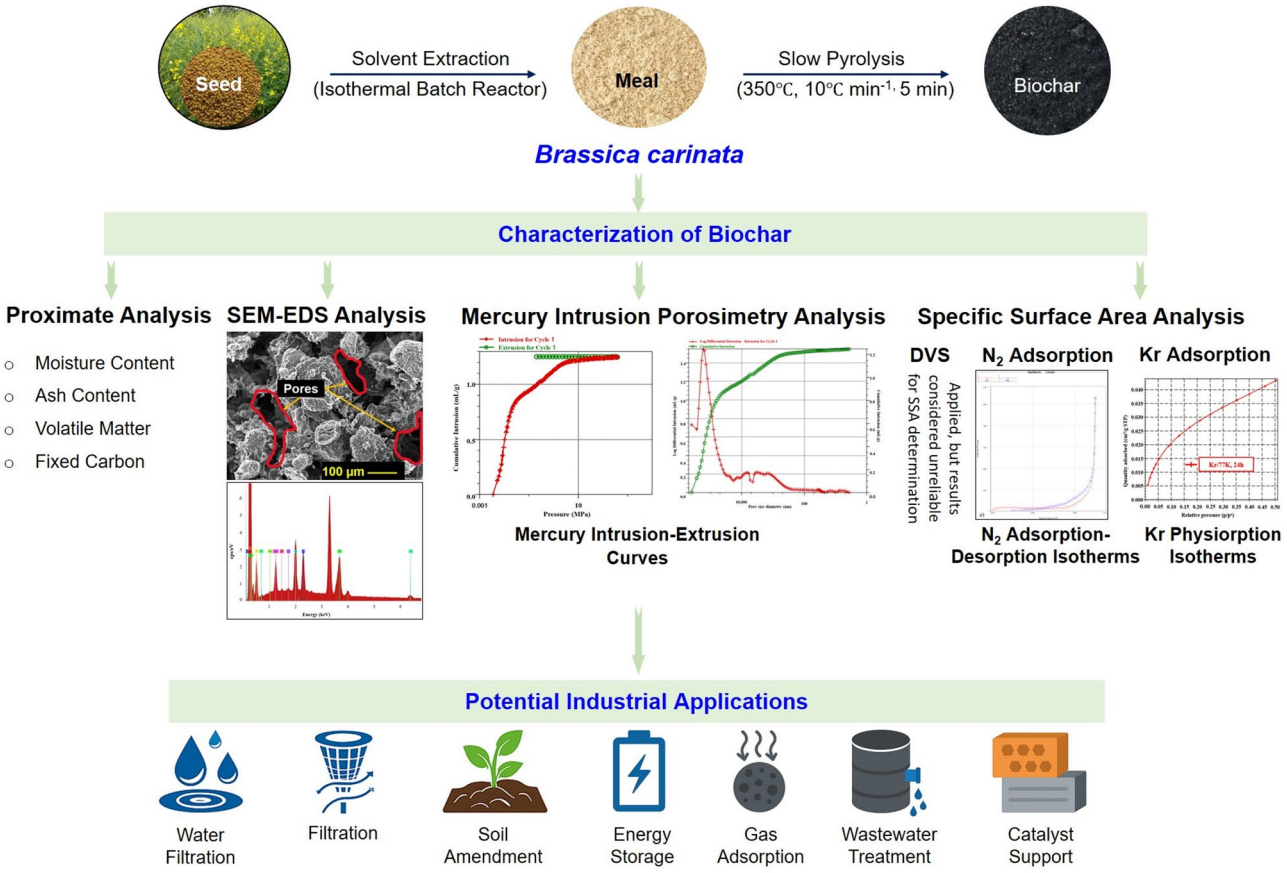

Fig. 9. Integrated scheme of the *B. carinata* biochar synthesis process, detailed physico-chemical characterization techniques, and assessment of potential industrial applications.

Conclusions

The present investigation employed multiple analytical approaches (proximate analysis, SEM-EDS, MIP, and gas adsorption techniques) to comprehensively characterize the physicochemical, structural, and textural qualities of the materials. This in-depth characterization primarily investigated biochars derived from two Ethiopian indigenous *B. carinata* species (Yellow Dodolla and Holetta-1), demonstrating their promising potential as a useful, carbon-rich material. Proximate analysis revealed that the biochars exhibited a volatile matter content ranging from 26 to 41 wt%, suggesting that material properties could be further enhanced through thermal devolatilization of the residual volatile matter. Furthermore, the analysis showed a total ash content of 11 to 15 wt.%, indicating that the inorganic mineral content is suitably preserved. This finding supports the biochars' promising potential as organic amendments in sustainable agriculture. Collectively, the biochars' favorable chemical composition profile [including K (1.32–1.49), Ca (0.76–0.78), Mg (0.36–0.39), Fe (0.02–0.11), P (0.48–0.64), and C (86), all in wt.%] and high stability (as indicated by the O/C ratio) represent useful properties that make them promising candidates for a variety of industrial applications.

Data availability

Data and materials are made available upon request to the corresponding author.

Received: 30 September 2025; Accepted: 8 December 2025
Published online: 09 February 2026

References

1. Kumar, A. et al. Multifaceted applications of Biochar in environmental management: A bibliometric profile. *Biochar* **5** (1), 11. https://doi.org/10.1007/s42773-023-00224-x (2023).
2. Hilioti, Z. et al. Characterization of castor plant-derived biochars and their effects as soil amendments on seedlings. *Biomass Bioenerg.* **105**, 96–106. https://doi.org/10.1016/j.biombioe.2017.07.009 (2017).
3. Wang, C. et al. Biochar-based slow-release of fertilizers for sustainable agriculture: A mini review. *Environ. Sci. Ecotechnology* 10. https://doi.org/10.1016/j.ese.2022.100155 (2022).
4. El-Naggar, A. et al. Biochar application to low fertility soils: A review of current status, and future prospects. *Geoderma* **337**, 536–554. https://doi.org/10.1016/j.geoderma.2018.10.033 (2019).
5. Irfan, M., Rafiullah, Kaleri, F., Rizwan, M. & Mehmood, I. Potential value of Biochar as a soil amendment: A review. *Pure Appl. Biology*. **6** (4), 1494–1502. https://doi.org/10.19045/bspab.2017.60017 (2017).

6. Hassan, M. & Carr, C. Biomass-derived porous carbonaceous materials and their composites as adsorbents for cationic and anionic dyes: A review. *Chemosphere* **265**, 129087. https://doi.org/10.1016/j.chemosphere.2020.129087 (2021).
7. Talaiekhozani, A., Rezania, S., Kim, K., Sanayeh, R. & Amani, A. Recent advances in photocatalytic removal of organic and inorganic pollutants in air. *J. Clean. Prod.* **278**, 123895. https://doi.org/10.1016/j.jclepro.2020.123895 (2021).
8. Bolan, N. et al. Multifunctional applications of Biochar beyond carbon storage. *Int. Mater. Rev.* **67** (2), 150–200. https://doi.org/10.1080/09506608.2021.1969408 (2022).
9. Senthil, C. & Lee, C. Biomass-derived Biochar materials as sustainable energy sources for electrochemical energy storage devices. *Renew. Sustain. Energy Rev.* **137**, 110464. https://doi.org/10.1016/j.rser.2020.110464 (2021).
10. Thomas, P., Lei, C. & Jethan, M. Recent developments in biomass-derived carbon as a potential sustainable material for supercapacitor-based energy storage and environmental applications. *J. Anal. Appl. Pyrol.* **140**, 54–85. https://doi.org/10.1016/j.jaap.2019.03.003 (2019).
11. Enaime, G., Baçaoui, A., Yaacoubi, A. & Lübken, M. Biochar for wastewater treatment-conversion technologies and applications. *Appl. Sci.* **10** (10), 1–29. https://doi.org/10.3390/app10103492 (2020).
12. Mishra, A. et al. Multidimensional approaches of biogas production and up-gradation: opportunities and challenges. *Bioresour. Technol.* **338**, 1–13. https://doi.org/10.1016/j.biortech.2021.125633 (2021).
13. Diacono, M., Persiani, A., Testani, E., Montemurro, F. & Ciaccia, C. Recycling agricultural wastes and by-products in organic farming: biofertilizer production, yield performance and carbon footprint analysis. *Sustainability* **11** (14), 1–17. https://doi.org/10.3390/su11143824 (2019).
14. Kandareli, R. et al. Cost effective and practically viable oil spillage mitigation: comprehensive study with Biochar. *Mar. Pollut. Bull.* **128**, 32–40. https://doi.org/10.1016/j.marpolbul.2018.01.002 (2018).
15. Zilberman, D., Laird, D., Rainey, C., Song, J. & Kahn, G. Biochar supply-chain and challenges to commercialization. *GCB Bioenergy*. **15** (1), 7–23. https://doi.org/10.1111/gcbb.12952 (2023).
16. Ding, Y. et al. Biochar to improve soil fertility: A review. *Agron. Sustain. Dev.* **36** (2). https://doi.org/10.1007/s13593-016-0375-x (2016).
17. de Medeiros, E. et al. Biochar as a strategy to manage plant diseases caused by pathogens inhabiting the soil: a critical review. *Phytoparasitica* **49** (4), 713–726. https://doi.org/10.1007/s12600-021-00898-w (2021).
18. Ahmad, M. et al. Biochar as a sorbent for contaminant management in soil and water: A review. *Chemosphere* **99**, 19–33. https://doi.org/10.1016/j.chemosphere.2013.10.071 (2014).
19. Wen, P. et al. Microwave-assisted synthesis of a novel biochar-based slow-release nitrogen fertilizer with enhanced water-retention capacity. *ACS Sustain. Chem. Eng.* **5** (8), 7374–7382. https://doi.org/10.1021/acssuschemeng.7b01859 (2017).
20. Chen, L. et al. Environmental-friendly montmorillonite-biochar composites: facile production and tunable adsorption-release of ammonium and phosphate. *J. Clean. Prod.* **156**, 648–659. https://doi.org/10.1016/j.jclepro.2017.04.053 (2017).
21. Batool, S., Idrees, M., Hussain, Q. & Kong, J. Adsorption of copper (II) by using derived-farmyard and poultry manure biochars: efficiency and mechanism. *Chem. Phys. Lett.* **689**, 190–198. https://doi.org/10.1016/j.cplett.2017.10.024 (2017).
22. Wystalska, K. & Kwarciak-Kozłowska, A. The effect of biodegradable waste pyrolysis temperatures on selected Biochar properties. *Materials* **14** (7), 1644. https://doi.org/10.3390/ma14071644 (2021).
23. Gul, S., Whalen, J. K., Thomas, B. W., Sachdeva, V. & Deng, H. Physico-chemical properties and microbial responses in biochar-amended soils: mechanisms and future directions. *Agric. Ecosyst. Environ.* **206**, 46–59. https://doi.org/10.1016/j.agee.2015.03.026 (2015).
24. Choudhury, I. & Hashmi, S. *Encyclopedia of Renewable and Sustainable Materials* pp. 370–378 (Elsevier, 2020).
25. Brewer, C. E. et al. New approaches to measuring Biochar density and porosity. *Biomass Bioenerg.* **66**, 176–185. https://doi.org/10.1016/j.biombioe.2014.03.018 (2014).
26. Sun, H., Hockaday, W., Masiello, C. & Zygourakis, K. Multiple controls on the chemical and physical structure of biochars. *Ind. Eng. Chem. Res.* **51** (9), 3587–3597. https://doi.org/10.1021/ie201309r (2012).
27. Keiluweit, M., Nico, P. S., Johnson, M. G. & Kleber, M. Dynamic molecular structure of plant biomass-derived black carbon (biochar). *Environ. Sci. Technol.* **44** (4), 1247–1253. https://doi.org/10.1021/es9031419 (2010).
28. Wildman, J. & Derbyshire, F. Origins and functions of macroporosity in activated carbons from coal and wood precursors. *Fuel* **70** (5), 655–661. https://doi.org/10.1016/0016-2361(91)90100-Y (1991).
29. Bird, M., Ascough, P., Young, I., Wood, C. & Scott, A. X-ray microtomographic imaging of charcoal. *J. Archaeol. Sci.* **35** (10), 2698–2706. https://doi.org/10.1016/j.jas.2008.04.018 (2008).
30. Sing, K. Reporting physisorption data for gas/solid systems with special reference to the determination of surface area and porosity (Recommendations 1984). *Pure Appl. Chem.* **57** (4), 603–619. https://doi.org/10.1351/pac198557040603 (1985).
31. Blankenship, L., Jagiello, J. & Mokaya, R. Confirmation of pore formation mechanisms in biochars and activated carbons by dual isotherm analysis. *Mater. Adv.* **3** (9), 3961–3971. https://doi.org/10.1039/D2MA00141A (2022).
32. Jagiello, J., Kenvin, J., Celzard, A. & Fierro, V. Enhanced resolution of ultra micropore size determination of biochars and activated carbons by dual gas analysis using N2 and CO2 with 2D-NLDFT adsorption models. *Carbon* **144**, 206–215. https://doi.org/10.1016/j.carbon.2018.12.039 (2019).
33. Rodríguez-Reinoso, F., Lopez-Gonzalez, J. D. & Berenguer, C. V. Activated carbons from almond shells—I: Preparation and characterization by nitrogen adsorption. *Carbon* **20** (6), 513–518. https://doi.org/10.1016/0008-6223(82)90001-3 (1982).
34. Qin, L., Xu, G., Yao, C. & Xu, Y. Conjugated microporous polymer networks with adjustable microstructures for high CO2 uptake capacity and selectivity. *Chem. Commun.* **52** (85), 12602–12605. https://doi.org/10.1039/C6CC05097B (2016).
35. Lapham, D. & Lapham, J. Gas adsorption on commercial magnesium stearate: the origin of atypical isotherms and BET transform data. *Powder Technol.* **342**, 676–689. https://doi.org/10.1016/j.powtec.2018.09.074 (2019).
36. Qin, L. et al. Joint analysis of pores in low, intermediate, and high rank coals using mercury intrusion, nitrogen adsorption, and nuclear magnetic resonance. *Powder Technol.* **362**, 615–627. https://doi.org/10.1016/j.powtec.2019.12.030 (2020).
37. Giesche, H. Mercury porosimetry: A general (practical) overview. *Part. Part. Syst. Charact.* **23** (1), 9–19. https://doi.org/10.1002/ppsc.200601009 (2006).
38. Hasanuzzaman, M., Rashid, A. & Olabi, A. G. Characterization of Porous Glass and Ceramics by Mercury Intrusion Porosimetry. In Reference Module in Materials Science and Materials Engineering. Elsevier. (2017). https://doi.org/10.1016/b978-0-12-803581-8.09459-0
39. Redda, Z. T., Laß-Seyoum, A., Yimam, A., Barz, M. & Jabasingh, S. Solvent extraction and characterization of *Brassica carinata* oils as promising alternative feedstock for bio-jet fuel production. *Biomass Conv Bioref.* **14**, 12207–12226. https://doi.org/10.1007/s13399-022-03343-x (2024).
40. Redda, Z., Laß-Seyoum, A., Yimam, A., Barz, M. & Jabasingh, S. Characterization of Hexane-Defatted brassica carinata oilseed meals to explore their potential for valorization towards a sustainable circular bioeconomy. *Waste Biomass Valoriz.* **15** (2), 1185–1197. https://doi.org/10.1007/s12649-023-02206-w (2024).
41. Redda, Z. et al. Pyrolysis-Based synthesis and characterization of Bio-Oil from brassica carinata oilseed meals and its application to produce Bio-Jet fuel. *Bioenergy Res.* **17** (2), 1328–1343. https://doi.org/10.1007/s12155-023-10657-z (2024).
42. Arvaniti, E. C. et al. Physical characterization methods for supplementary cementitious materials. *Mater. Struct.* **48**, 3675–3686. https://doi.org/10.1617/s11527-014-0466-4 (2015).

43. Groen, J. C., Peffer, L. A. & Pérez-Ramírez, J. Pore size determination in modified micro- and mesoporous materials. Pitfalls and limitations in gas adsorption data analysis. *Microporous Mesoporous Mater.* **60** (1–3), 1–17. https://doi.org/10.1016/S1387-1811(03)00335-5 (2003).
44. Malm, L., Danielsson, A., Sand, A., Rosenkranz, J. & Ymén, I. Application of dynamic vapor sorption for evaluation of hydrophobicity in industrial-scale froth flotation. *Miner. Eng.* **127**, 305–311. https://doi.org/10.1016/j.mineng.2017.08.019 (2018).
45. Nanda, S. et al. Characterization of North American lignocellulosic biomass and biochars in terms of their candidacy for alternate renewable fuels. *Bioenergy Res.* **6** (2), 663–677. https://doi.org/10.1007/s12155-012-9281-4 (2013).
46. Hadey, C., Allouch, M., Alami, M., Boukhlifi, F. & Loulidi, I. Preparation and characterization of biochars obtained from biomasses for combustible briquette applications. *Sci. World J.* **2022** https://doi.org/10.1155/2022/2564475 (2022).
47. Zhou, B. et al. Effect of pyrolysis temperature, heating rate, and residence time on rapeseed stem derived Biochar. *J. Clean. Prod.* **174**, 977–987. https://doi.org/10.1016/j.jclepro.2017.11.05 (2018).
48. Angın, D. & Şensöz, S. Effect of pyrolysis temperature on chemical and surface properties of Biochar of rapeseed (*Brassica Napus* L). *Int. J. Phytoremediation*. **16** (7–8), 684–693. https://doi.org/10.1080/15226514.2013.85684 (2014).
49. Choudhary, T., Khan, K., Hussain, Q., Ahmad, M. & Ashfaq, M. Feedstock-induced changes in composition and stability of Biochar derived from different agricultural wastes. *Arab. J. Geosci.* **12** (12), 1–13. https://doi.org/10.1007/s12517-019-4796-z (2019).
50. Aziz, M. Z., Naveed, M., Abbas, T., Siddique, S. & Yaseen, M. Alternative fertilizers and sustainable agriculture. In *Innovations in Sustainable Agriculture* (eds Farooq, M. & Pisante, M.) (Springer, 2019). https://doi.org/10.1007/978-3-030-23169-9_8.
51. Abebe, T. G., Tamtam, M. R., Abebe, A. A., Abtemariam, K. A. & Shigut, T. G. Growing use and impacts of chemical fertilizers and assessing alternative organic fertilizer sources in Ethiopia. *Appl. Environ. Soil. Sci.* https://doi.org/10.1155/2022/4738416 (2022).
52. Wijitkosum, S. & Jiwnok, P. Elemental composition of Biochar obtained from agricultural waste for soil amendment and carbon sequestration. *Appl. Sci.* **9** (19), 3980. https://doi.org/10.3390/app9193980 (2019).
53. Jindo, K., Mizumoto, H., Sawada, Y., Sanchez-Monedero, M. & Sonoki, T. Physical and chemical characterization of biochars derived from different agricultural residues. *Bioresources* **11** (23), 6613–6621. https://doi.org/10.5194/bg-11-6613-2014 (2014).
54. Uchimiya, S. et al. Evaluation of plant-based activated carbons and agricultural residues as adsorbents for the removal of cations and anions from aqueous solutions. *J. Environ. Qual.* **40** (6), 1957–1965. https://doi.org/10.2134/jeq2011.0097 (2011).
55. Almutairi, A., Ahmad, M., Rafique, M. & Al-Wabel, M. I. Variations in composition and stability of biochars derived from different feedstock types at varying pyrolysis temperature. *J. Saudi Soc. Agricultural Sci.* **22** (1), 25–34. https://doi.org/10.1016/j.jssas.2022.05.003 (2023).
56. Masiello, C. A. et al. Biochar effects on soil hydrology. In Biochar for environmental management (2nd ed., pp. 541–560). Routledge. (2015). https://doi.org/10.4324/9780203762264
57. Tomczyk, A., Sokolowska, Z. & Boguta, P. Biochar physicochemical properties: pyrolysis temperature and feedstock kind effects. *Reviews Environ. Sci. Bio/Technology*. **19** (19), 191–215. https://doi.org/10.1007/s11157-020-09523-y (2020).
58. Shaaban, A. et al. Influence of heating temperature and holding time on biochars derived from rubber wood sawdust via slow pyrolysis. *J. Anal. Appl. Pyrol.* **107**, 31–39. https://doi.org/10.1016/j.jaap.2014.01.017 (2014).
59. Thommes, M. et al. Physisorption of gases, with special reference to the evaluation of surface area and pore size distribution (IUPAC technical Report). *Pure Appl. Chem.* **87** (9-10), 1051–1069. https://doi.org/10.1515/pac-2014-1117 (2015).
60. Sing, K. The use of nitrogen adsorption for the characterisation of porous materials. *Colloids Surf., A*. 187–188. https://doi.org/10.1016/S0927-7757(01)00612-4 (2001).
61. Thommes, M., Morell, J., Cychosz, K. & Fröba, M. Combining nitrogen, argon, and water adsorption for advanced characterization of ordered mesoporous carbons (CMKs) and periodic mesoporous organosilicas (PMOs). *Langmuir* **29** (48), 14893–14902. https://doi.org/10.1021/la402832b (2013).
62. Nopens, M. et al. Determination of mesopores in the wood cell wall at dry and wet state. *Sci. Rep.* **10** (1), 1–11. https://doi.org/10.1038/s41598-020-65345-0 (2020).
63. Maziarka, P. et al. Do you BET on routine? The reliability of N2 physisorption for the quantitative assessment of biochar's surface area. *Chem. Eng. J.* **418**, 129234. https://doi.org/10.1016/j.cej.2021.129234 (2021).
64. International Organization for Standardization. ISO 9277: Determination of the specific surface area of solids by gas adsorption using the BET method. (2010).

Acknowledgements

Zinnabu Tassew Redda wishes to express his profound gratitude to all Faculty I colleagues at HTW Berlin and to Dr. Özge Mutlu of the German Biomass Research Centre (DBFZ), Leipzig, for facilitating access to the N2 adsorption study. Additionally, sincere appreciation is extended to Mrs. Annett Zimathies and colleagues within the Department of Structural Analysis at Federal Institute for Materials Research and Testing (BAM), Berlin, for their critical assistance and facilitation of the DVS, MIP, and Kr adsorption laboratory procedures.

Author contributions

ZTR contributed to the conceptualization, formal analysis, investigation, writing—original draft, writing—review & editing. Supervision by AL-S, AY, and MB. ZTR and CP performed the design of methods, execution of experiments, and analysis of results. AL-S additionally supervised resource utilization and project administration. KB contributed to the execution of experiments for SEM-EDS analysis. DGG contributed to writing—review & editing. The final manuscript has been reviewed and approved by all authors.

Funding

The Faculty I, University of Applied Sciences (HTW), Berlin, Germany, provided the whole technical support, for which the author, Zinnabu Tassew Redda, would like to express his heartfelt gratitude. The author would also like to express his profound gratitude to the Structural Analysis Department, Federal Institute for Materials Research and Testing (BAM), Berlin, Germany for the technical assistance provided by the department; as well as the technical and financial support provided by Addis Ababa University, Addis Ababa, Ethiopia (grant number: Ph.D. RG-GSR/1466/10).

Declarations

Competing interests

The authors declare no competing interests.

Additional information

Supplementary Information The online version contains supplementary material available at https://doi.org/10.1038/s41598-025-32063-1.

Correspondence and requests for materials should be addressed to Z.T.R.

Reprints and permissions information is available at www.nature.com/reprints.

Publisher's note Springer Nature remains neutral with regard to jurisdictional claims in published maps and institutional affiliations.